

Graptolite-Derived Organic Matter and Pore Characteristics in the Wufeng-Longmaxi Black Shale of the Sichuan Basin and its Periphery



WU Jin^{1,2,3,4,*}, ZHOU Wen¹, SUN Shasha^{2,3,4}, ZHOU Shangwen^{2,3,4} and SHI Zhensheng^{2,3,4}

¹ State Key Laboratory of Oil and Gas Reservoir Geology and Exploitation, Chengdu University of Technology, Chengdu 610059, Sichuan, China

² Research Institute of Petroleum Exploration and Development, PetroChina, Beijing 100083, China

³ National Energy Shale Gas R&D (Experiment) Centre, Langfang 065007, Hebei, China

⁴ PetroChina Unconventional Oil & Gas Key Laboratory, Langfang 065007, Hebei, China

Abstract: A key target of shale gas exploration and production in China is the organic-rich black shale of the Wufeng Formation-Longmaxi Formation in the Sichuan Basin and its periphery. The set of black shale contains abundant graptolites, which are mainly preserved as flattened rhabdosomes with carbonized periderms, is an important organic component of the shale. However, few previous studies had focused on the organic matter (OM) which is derived from graptolite and its pore structure. In particular, the contributions of graptolites to gas generation, storage, and flow have not yet been examined. In this study, focused ion beam-scanning electron microscope (FIB-SEM) was used to investigate the characteristics of the graptolite-derived OM and the micro-nanopores of graptolite periderms. The results suggested that the proportion of OM in the graptolite was between 19.7% and 30.2%, and between 8.9% and 14.4% in the surrounding rock. The total organic carbon (TOC) content of the graptolite was found to be higher than that of the surrounding rock, which indicated that the graptolite played a significant role in the dispersed organic matter. Four types of pores were developed in the graptolite periderm, including organic gas pores, pyrite moulage pores, authigenic quartz moldic pores, and micro-fractures. These well-developed micro-nano pores and fractures had formed an interconnected system within the graptolites which provided storage spaces for shale gas. The stacked layers and large accumulation of graptolites resulted in lamellation fractures opening easily, and provided effective pathways for the gas flow. A few nanoscale gas pores were observed in the graptolite-derived OM, with surface porosity lie in 1.5%–2.4%, and pore diameters of 5–20 nm. The sapropel detritus was determined to be rich in nanometer-sized pores with surface porosity of 3.1%–6.2%, and pore diameters of 20–80 nm. Due to the small amount of hydrocarbon generation of the graptolite, supporting the overlying pressure was difficult, which caused the pores to become compacted or collapsed.

Key words: graptolite, pore structure, shale gas, Wufeng-Longmaxi Formations, Sichuan Basin

Citation: Wu et al., 2019. Graptolite-Derived Organic Matter and Pore Characteristics in the Wufeng-Longmaxi Black Shale of the Sichuan Basin and its Periphery. Acta Geologica Sinica (English Edition), 93(4): 982–998. DOI: 10.1111/1755-6724.13860

1 Introduction

Graptolites are the most commonly observed fossils in Lower Paleozoic (Ordovician-Lower Devonian) marine sediment. The majority of the Ordovician and Silurian graptolites are planktonic types which sank down the seafloor after death, and were buried layer upon layer in deep water mudstone (Suchý et al., 2003; Gupta et al., 2006; Zhang et al., 2008; Tenger et al., 2017; Zou et al., 2015, 2019). Graptolites are known to lack biomineralized skeleton, and pyrite may preserve the 3D morphology by growing as an infill under certain circumstances. However, the graptolite periderm is routinely preserved as organic material, and the zooids were normally decayed before burial (Bjerreskov, 1991; Underwood and Bottrell 1994; Gupta et al., 2006). The organic-rich shale of the Wufeng-Longmaxi Formation (WF-LMX Fm) in the

Sichuan Basin, along with the periphery, are considered to be a set of high-quality marine hydrocarbon source rock with a main shale gas producing layer (Zou et al., 2015, 2016; Ma, 2017; Dong et al., 2018; Liu et al., 2018; Zhai et al., 2018). Abundant graptolites (periderm) have been observed in the WF-LMX Fms, which were observed to be stacked along the shale lamellation (Chen et al., 2000, 2005; Nie et al., 2017; Wu et al., 2017; Zou et al., 2018). In recent years, with the large-scale exploration and development of shale gas in the WF-LMX Fm, increasing amounts of attention have been given to the ubiquitous graptolites in the aforementioned shale set. The basic problems, such as the contribution to the total OM and the hydrocarbon generation capacity of the graptolite fauna, have consistently plagued petroleum geologists in previous explorations.

The results of the previous studies have suggested that alginite and zooclasts (graptolites) were the most common

* Corresponding author. E-mail: wujinouc@petrochina.com.cn

organic constituents in the high-quality shale interval of the WF-LMX Fm (Shen et al., 2016; Tenger et al., 2017). For example, Suchý et al. (2003) believed that graptolite macerals were the most ubiquitous and volumetrically predominant microscopic organic components of the shale. Also, Petersen et al. (2013) considered that graptolite fragments formed the most abundant organic components in the lower Paleozoic shales of southern Scandinavia, and identified the dominant contribution of the graptolites to the dispersed OM. Luo et al. (2015) observed that graptolite fragments accounted for 20% to 93% of the dispersed OM in the LMX Fm. However, the contribution of the graptolite-derived OM to the total OM in the WF-LMX Fm has not yet been studied systematically.

Graptolites are an extinct class of colonial marine organisms (Gupta et al., 2006). Towe and Urbanek (1972) and Crowther et al. (1981) utilized electron microscopy to study the ultrastructures of graptolites periderm. The results revealed that the original composition was composed of collagen and polysaccharide. Using infrared spectroscopy, Bustin et al. (1989) demonstrated that graptolite periderm was primarily comprised of aromatic structures with aliphatic groups. Furthermore, the results of the pyrolysis analysis conducted by Rock-Eval suggested the hydrogen and oxygen indices of the graptolite periderms were similar to Type II kerogen, and were found to exhibit a progressive decrease in hydrogen index with increasing maturation. Briggs et al. (1995) considered that the graptolite periderm was a highly altered kerogen-like substance rich in aliphatic biomacromolecules. In another related study, using in situ polymerization, Gupta et al. (2006) concluded that the aliphatic composition of the graptolite periderm reflected the direct incorporation of lipids from the organism itself. Shen et al. (2016) conducted Py-GC analyses of graptolites extracted from the Wufeng-Longmaxi Fm and determined that the hydrocarbon products were mainly gaseous hydrocarbons and light oils. These results illustrated that the chemical composition of the graptolite periderm was dominated by aliphatic components. The present study considered that the graptolite periderm was mainly composed of aliphatic components similar to Type II kerogen, in which the hydrocarbon products are mainly gaseous hydrocarbons. These findings indicated that graptolites could potentially be a good hydrocarbon-generating material at low maturation. Therefore, during its long geological history, complex micro-nano pores may have been developed on the graptolite periderm. The development of the organic gas pores may potentially reflect the hydrocarbon-generating abilities of the graptolite. However, there have been few studies conducted regarding the development characteristics of micro-nanopores on the periderm of graptolites. In previous related research studies, Dai et al. (2015), Ma et al. (2016), Zhou et al. (2017), and Nie et al. (2018) observed that nanoscale organic pores were locally developed on the graptolite periderm in the WF-LMX black shale of the Jiaoshiba region. However, the classification and origin of these organic pores have not currently been established. In addition, how the organic

pores in the graptolites affect the accumulation and seepage of shale gas requires further systematic study. In summary, due to insufficient study results, the understanding of the contributions of graptolites to the formation and storage of shale gas remains unclear.

In the current study, graptolite-bearing shale samples were selected from the WF-LMX Fm in the Sichuan Basin and its periphery. Then, qualitative and quantitative analyses of the contributions of the graptolite-derived OM to the total OM were conducted using Benchtop-SEM and TOC analysis methods, respectively. Meanwhile, the pore structures of the graptolite were illustrated using FIB-SEM, and how different pore types contributed to the shale gas accumulations and effective flow pathways were discussed. Finally, a gallium beam method was used to vertically cut a graptolite body in order to observe its internal organic gas pore development. In this studies summary, the hydrocarbon generation capacity of the graptolite-derived OM, as well as its contribution to the gas content of the shale, were detailed. The results of this research study clearly illustrated the contributions of the graptolite-derived OM to the WF-LMX shale reservoirs, and potentially provided a theoretical foundation for future shale gas explorations in southern China.

2 Samples and Experiments

2.1 Geological setting and samples

The Sichuan Basin is located in the eastern section of Sichuan Province and Chongqing Municipality, and reaches to Longmen Mountain in the west; Qiyue Mountain in the east; Micao Mountain-Daba Mountain in the north, and Daliangshan-Laoshan in the south. This study included the two anticlinal belts of Huayingshan and Longquanshan as the boundaries, and divided the Sichuan Basin into three tectonic units as follows: the area located east of Huaying Mountain is a high and steep tectonic zone of the Southeast Sichuan Slope, and includes the high steep folds of eastern Sichuan and the low steep folds of southern Sichuan; and the area located west of Longquanshan is a low steep structural area within the West Sichuan Depression, between the low-gentle structural zone of the Central Sichuan Uplift, as detailed in Fig. 1. During the Late Ordovician period, with the occurrence of the Caledonian tectonic movements, the collision actions between the Yangtze and Cathaysia blocks were intensified. As a result, marginal uplifts were formed, such as the Central Sichuan Uplift, Central Guizhou Uplift, and the Xuefeng Uplift. This led to restricted shallow water areas surrounded by uplifts, and asedimentary environment characterized by low-energy, under-compensation, and anoxic conditions (Gao et al., 2014a; Mu et al., 2014; Ran et al., 2016; Zou et al., 2015; Nie et al., 2017; Li et al., 2018). Then, affected by tectonic movements and two large-scale global transgressions, a set of thin siliceous shale layers was deposited during the Late Ordovician WF Fm, which contained abundant graptolites, such as *Amplexograptus*, *Dicellograptus*, *Tangyagraptus*, and *Diceratograptus* (Chen et al., 2000, 2005; Wang et al., 2015; Nie et al., 2017). The Lower Silurian LMX Fm was characterized by black organic rich shale deposits with

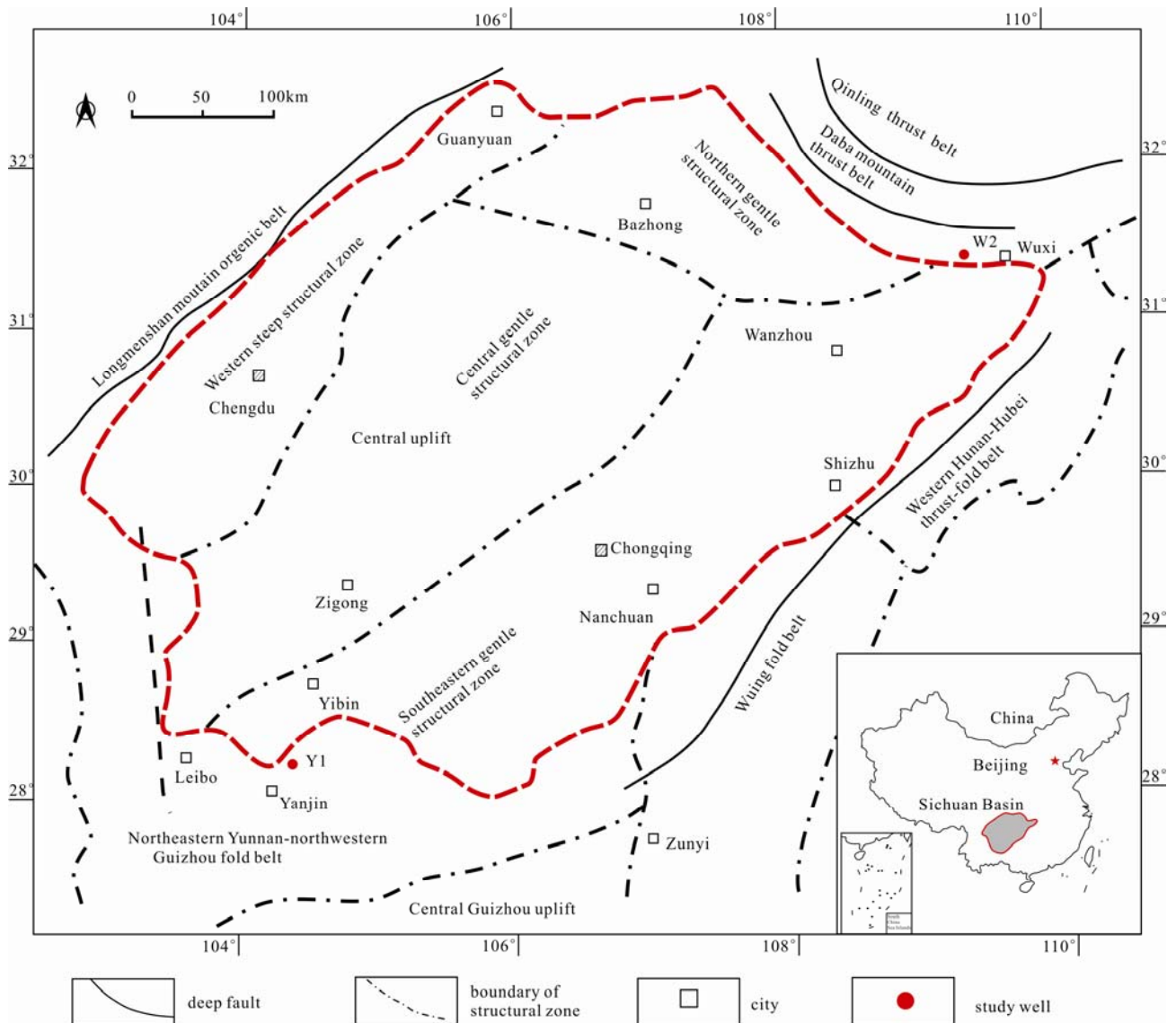


Fig. 1. Tectonic units and locations of the examined wells in the periphery of the Sichuan Basin in the southern China (modified from Zhao et al., 2017).

China basemap after China National Bureau of Surveying and Mapping Geographical Information.

abundant graptolites, such as *Glyptograptus*, *Parakidograptus*, *Cystograptus*, *Demirastrites*, *Lituigraptus*, and *Stimulograptus* (Chen et al., 2000; Wang et al., 2015; Nie et al., 2017).

The study areas were located in the Wuxi area of the northeastern Sichuan Basin and the Yanjin area of the southern Sichuan Basin. The graptolite-bearing shale samples were selected from the lower Longmaxi and Wufeng shale section in Well Wuxi #2 (WX2) and Well Yanjin #1 (YJ1), as shown in Fig. 1. The target intervals of the two wells were mainly composed of carbonaceous mudstone, carbonaceous shale, and siliceous shale. The parallel beddings were observed to be well developed, and a large number of graptolite fossils were stacked along the bedding surface. Chen et al. (2015) had previously established the graptolite zone sequence of the WF-LMX Formation in the Yangtze area, which was used in this

study as the standard for the stratigraphic division and comparison of the black shale. The Upper Ordovician formation consisted of Katian (WF1, WF2, and WF3 biozones) and Hirnantian (WF4 and LM1 biozones). Meanwhile, it was determined that the late stage of the Katian to the early stage of the Hernandian corresponded to the depositional period of the Wufeng Formation and Guanyinqiao Member. The Llandovery mainly included Rhuddanian (LM2, LM3, LM4, and LM5 biozones); Aeronian (LM6, LM7, and LM8 biozones); and Telychian (LM9/N1 and N2 biozones). The lower part of the Llandovery was referred to as the Longmaxi Formation of the Upper Yangtze area. The detailed identification of the graptolites in Well WX2 and Well YJ1 indicated that the WF-LMX Fm of the two wells had twelve graptolite biozones and eight graptolite biozones developed, respectively. In this study, a total of ten shale samples

were selected from the Katian, Rhuddanian, and Aeronian biozones. The detailed information regarding these samples, such as the depths, biozones, and TOC content, are illustrated in Table 1.

2.2 Experimental methods

In this study, Benchtop-SEM, FIB-SEM, and geochemical analyses were performed in order to assess the contributions of the graptolite-derived OM to the total OM, and to also depict the development characteristics of the OM-pores in the graptolites. In order to avoid damaging the thin film of the graptolite, the microstructures of the graptolites were observed within the core intersection, and then the same surface layer was polished in order to more clearly conduct observations of the OM in the surrounding rock (sapropelinite). Using this method, a comparative and accurate analysis could be carried out. Then, for the purpose of quantifying the pore spaces shown in the SEM images, several representative high-resolution images were processed using Image Avizo Fire 8.0 software. This type of software has recently been applied to quantitatively analyze the porosity in gray-scale SEM images due to its high accuracy and efficiency results. All of the aforementioned experiments were carried out at the National Energy Shale Gas Research and Development (Experimental) Center.

2.2.1 TOC analysis process

It has been found that TOC analysis is an effective method for determining total organic carbon content. In this study, crushed shale samples were soaked in a 5% HCl solution for two days for the purpose of removing the carbonates. The samples were then dried in a stoving oven at 65°C for two days. After that, the TOC content was measured using a LECO CS-200 carbon and sulfur analyzer, with the accuracy controlled to within 0.5%.

2.2.2 SEM observational process

In this research study, shale samples with complete graptolites on the bedding surface were selected to be cut in the vertical direction, and appropriate sized blocks were achieved. The samples were mounted to SEM stubs with carbon tape, and then coated with carbon to provide a conductive surface layer. In order to determine the positions of the graptolites, a Benchtop-SEM method under the low resolution was used for a comparison analysis with optical photographs. Then, the macroscopic structural characteristics of the graptolites were observed in a backscatter electron (BSE) mode, and the distribution of the graptolite-derived OM was clearly defined. At this point, energy dispersive spectroscopy analyses of the graptolite fragments were conducted in order to identify the composition of the elements. Subsequently, the surfaces were polished using dry emery paper, the distribution of the OM in the sapropel detritus was observed within the same field of view.

2.2.3 FIB-SEM slicing and imaging process

In this study, SEM observations and three-dimensional “Slices of Samples” were performed using an FEI Helios NanoLab™ 650 DualBeam™ FIB-SEM with a resolution

of 0.8 nm. The system consisted of two beams, an electron beam and an ion beam, and there was an angle of 52° between the beams. First of all, the prepared samples were placed into a sample chamber and vacuumed. Then, the electron beam was opened, and the working distance was adjusted to 4 mm. At that point, the electron gun was vertical to the surfaces of the samples, and the two-dimensional microstructures of the OM could be clearly observed. The backscatter electron (BSE) and secondary electron (SE) imaging modes were alternately performed in order to observe the micro-nanopores on the graptolite periderm. The BSE mode is biased toward delineating compositional variations, therefore is often used to identify minerals. Due to the high resolution and stereoscopic effects of SE images, these images are often acquired for observing topographic variations and identifying pores. Therefore, it was possible in this study to accurately determine the positions of the graptolite fragments, and to select the areas of interest. Then, the pore shapes, sizes, and distributions, along with connectivity of the graptolite nanoporosity, were observed in the SE mode. Subsequently, the electron and ion beams were simultaneously turned on and the samples were rotated 52°, so that the ion gun was vertical to the sample surfaces. Platinum (Pt) was then coated over the areas of interest in order to minimize curtaining artifacts on the milled shale surfaces. A focused 30 kV beam of gallium ions was able to continuously mill the samples by sputtering away the shale material. During the continuous milling and imaging, Slice&View software was used to manipulate the FIB-SEM, with the thicknesses of each sheet set as 10 nm. Finally, the SEM images of the newly milled shale surfaces had achieved a resolution of 2.5 nm at 2 kV accelerating voltage, and the working distance was approximately 4.0 mm.

3 Results

3.1 Distribution of the TOC

In the study area, Well WX2 was located in the Wuxi area of the northeastern Sichuan Basin. The depths of the target intervals of the Wufeng Formation and Longmaxi Formation were between 1,510.41 m and 1,637.5 m. The organic-rich shale (TOC>2%) extended from the Katian to the middle and lower sections of the Telychian, with thicknesses of approximately 89.8 m. The TOC content ranged from 0.19% to 7.3%, with an average of 2.7%. The TOC content was observed to gradually increase from the top to the bottom. The OM abundance of the graptolite shale interval LM1-LM3 at the bottom of the Longmaxi Formation was found to be the highest, with a TOC content of between 3.1% and 7.3%, and an average of 5.6% (Fig. 2a). Well YJ1 was located in the Yanjin area of the southern Sichuan Basin in the study area. The depths of the target intervals of the Wufeng Formation and Longmaxi Formation ranged from 1,315.68 m to 1,546.7 m, and the thickness of the organic-rich shale (TOC>2%) was approximately 38 m. The distributions of the TOC content ranged from 0.58% to 8.6%, with an average of 2.2%. When compared with the distribution trend of the TOC content in Well WX2, the TOC content of Well YJ1

also displayed a gradual increasing trend from the top to the bottom. The TOC content of the graptolite shale interval LM1-LM3 was determined to be highest, with a TOC content of between 2.6% to 8.6%, and an average of 5.27% (Fig. 2b).

In this study, it was found that the graptolite fauna had experienced radiation, step-wise mass extinctions, recovery events, and re-radiation during the Ordovician and Silurian period transition on the Yangtze platform (Chen et al., 2004; Chen et al., 2005). Furthermore, it was determined that there had been a small radiation event in the *D.complexus* Zone to the *T.typicus* Zone (WF2 to WF3b). This was observed to be the last radiation event of the ordovician graptolite fauna. During that period, the abundance of graptolites was higher (Fig. 3a). A major extinction event in the Yangtze region occurred in the upper-*P.pacificus* Zone to the middle *N.extraordinarius-N.ojsuenensis* Zone (WF3c to WF4). Ashgill DDO fauna was determined to be the highest diversity Ordovician graptolite fauna, the majority of which was truncated by the major extinction event, which subsequently resulted in the lowest abundance of graptolites. It was also found that a recovery of graptolite fauna had occurred from the upper *N.extraordinarius-N.ojsuenensis* Zone to the upper *N.persculptus* Zone (WF4 to LM1), which gave rise to many new species. Subsequently, from the upper *N.persculptus* Zone to the *A.ascensus* Zone (LM1 to LM3), several disaster species may have covered the entire bedding surface in high abundance (Chen et al., 2005a). The disaster species, which may have occupied

the ecological space left empty by the extinction of the DDO fauna, were characterized by a monospecific bedding plane occurrence (Chen et al., 2005a.b), as illustrated in Fig 3b. During this period, the graptolites were believed to be numerically abundant. The core observations and TOC analysis indicated that the TOC content of Well WX2 and Well YJ1 were coincidental with the step-wise mass extinctions, recovery events, and re-radiation events. The graptolite shale interval LM1-LM3 had the highest graptolite abundance corresponding to the highest TOC content (Fig. 2). Generally speaking, there was a positive correlation observed between the graptolite abundance and TOC content in the black shale of the study area.

3.2 Elemental composition of the graptolite

The plankton graptolites lacked biomineralized skeletons, and were mainly preserved as combinations of carbonized skeletal material (periderm) stacked along the bedding surfaces. The majority of the kerogenization graptolite fossils (fossilized organisms) preserved the outlines of the living graptolites. The macroscopic morphological features of the graptolites could be clearly observed using a Benchtop-SEM (Figs. 4a, 4d) method. The macrostructures of the graptolite, such as the thecal apertures and interthecal septums, were observed using a BSE method. The fragments of the graptolite-derived OM were found to be distributed as sheets, with different sizes and poorly preserved fine structures (Figs. 4b, 4e). This study performed energy dispersive spectroscopy (EDS) in

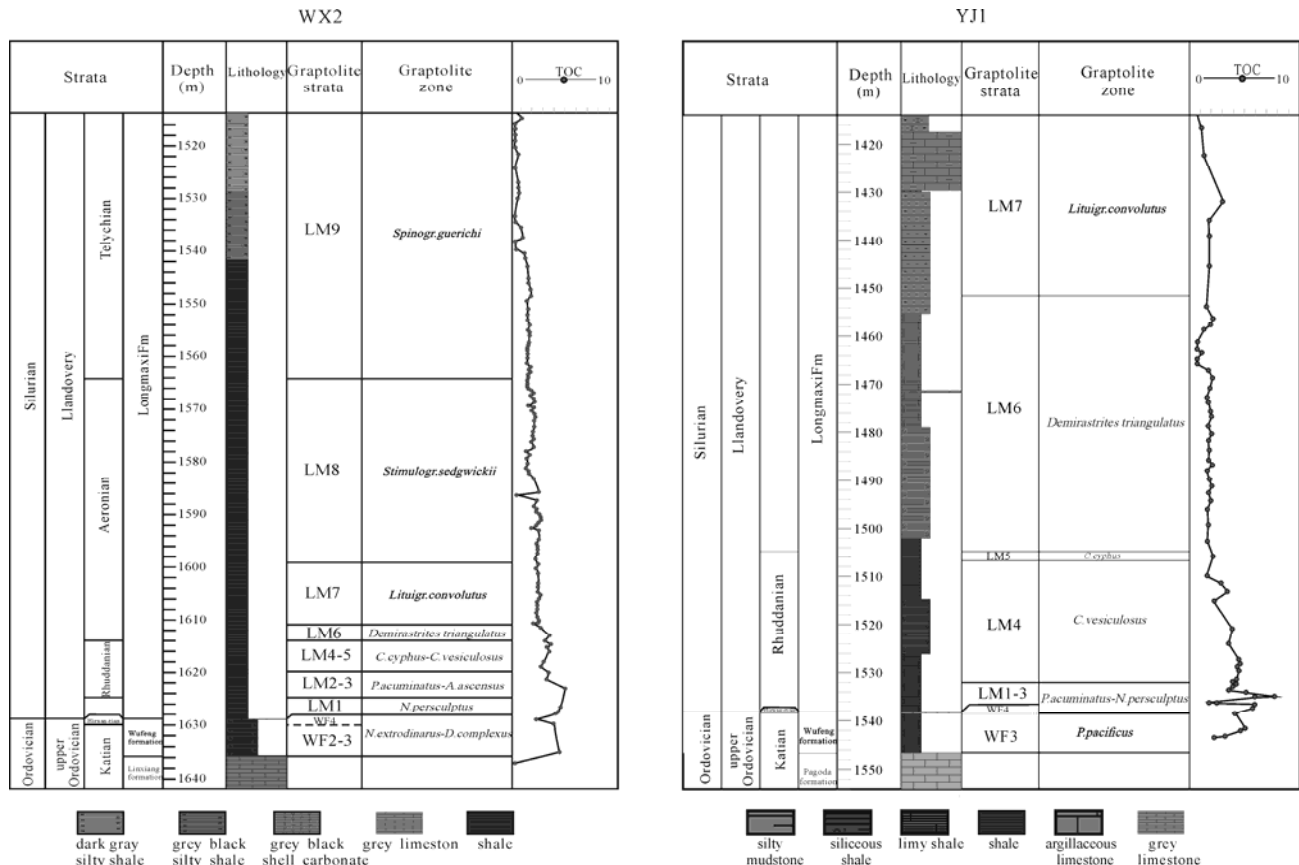


Fig. 2. Comprehensive stratigraphic column of the shale reservoirs of the examined two wells: (a) Well WX2; (b) Well YJ1.

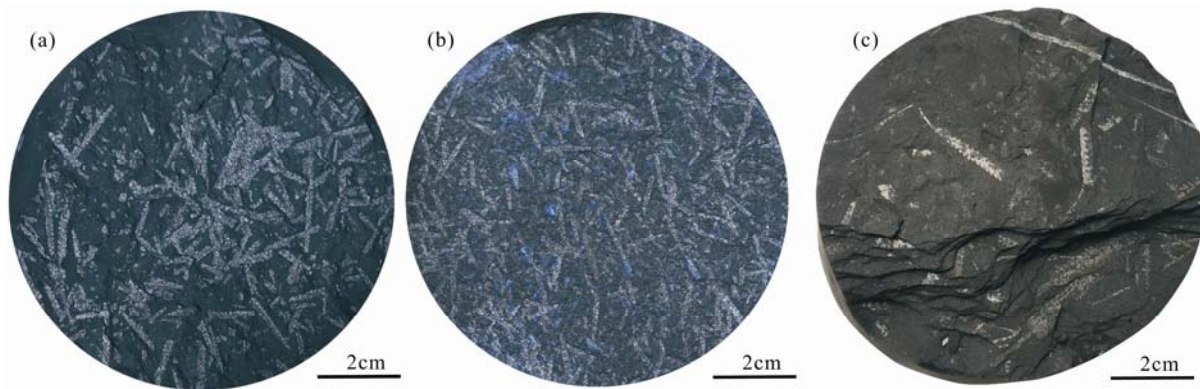


Fig. 3. Typical graptolite-bearing shale.

(a) Large number of graptolites developed in shale interval WF2 to WF3b of well YJ1-01; (b) disaster species covering the entire bedding surface in high abundance in shale interval LM2 to LM3 of well YJ1-05; (c) graptolite-bearing shale with subtle bedding structure and large amounts of graptolites in the lamellar distribution of well YJ1-05.

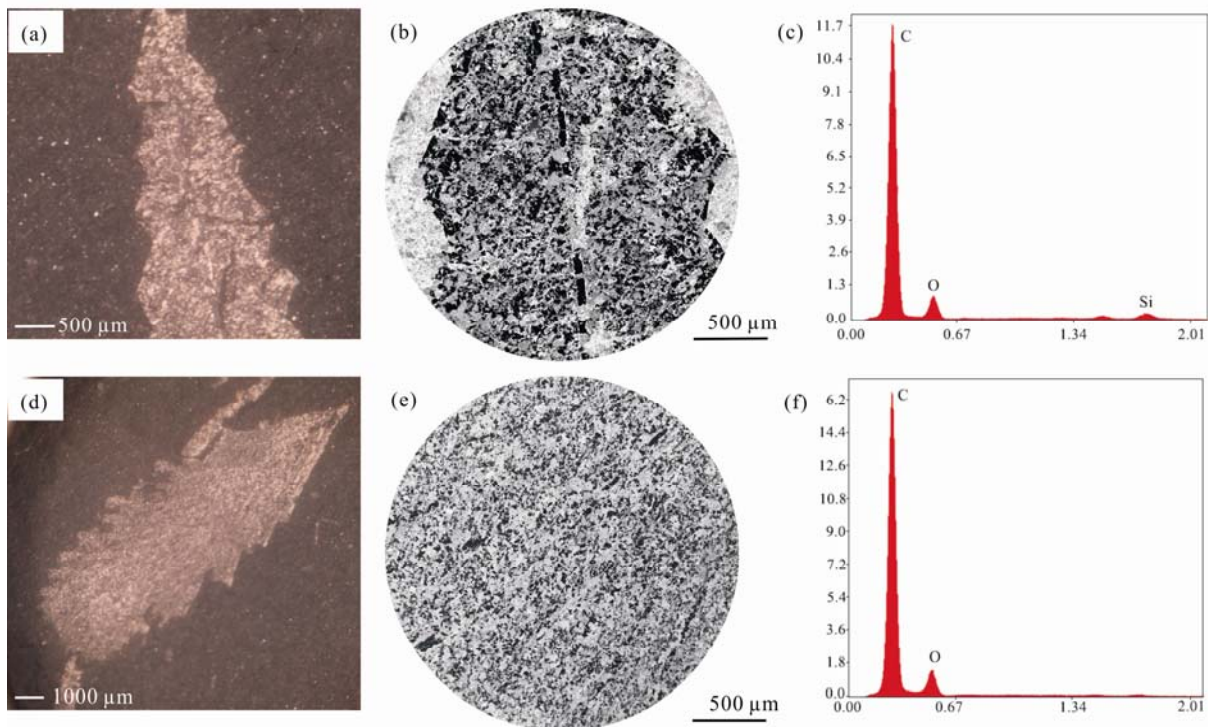


Fig. 4. Macro-morphology and element composition analyses of the graptolites.

(a) Benchtop-SEM images showing the macromorphology of the graptolite in WX2-05; (b) macrostructure of the graptolite under BSE showing thecal apertures and intertheal septums, with the graptolite fragments distributed as sheets in WX2-05; (c) EDS revealing element compositions of the graptolite fragments in WX2-05; (d) macromorphology of the graptolite in WX2-04; (e) graptolite fragments distributed as sheets, with poorly preserved fine structures under BSE in WX2-04; (f) EDS revealing element compositions of the graptolite fragments in WX2-04.

situ in order to accurately identify of the composition of the elements in the graptolite-derived OM. The results showed that the graptolite-derived OM were composed of carbon, oxygen, and silicon elements, among which the content of carbon was found to be the highest, accounting for between 85% to 95%. These findings indicated that the organic material was the predominant composition of the graptolite fragments.

3.3 Pore micro-structures of the graptolites obtained using FIB-SEM imaging

The detailed FIB-SEM observations confirmed that a

large number of micro-nanometer pores were developed in the graptolite periderm, which could be divided into four categories as follows: organic gas pores; pyrite moulage pores; authigenic quartz moldic pores; and micro-fractures.

3.3.1 Framboidal pyrite moulage pores

It was known that the graptolites had sank to seafloor after death, and the zooids were decomposed by the sulfate-reducing bacteria to produce hydrogen sulfide (H_2S), which then reacted with dissolved iron from the surrounding areas to form iron monosulfide. The iron

monosulfide were eventually transformed into framboidal pyrite which precipitated on the graptolite periderm (Briggs et al. 1991, 1996; Schieber, 2002; Wilkin, 1997; Baliński and Sun 2013). In addition, due to the degradation of the soft tissues, a reducing micro-environment was formed around the graptolites, which was beneficial to the formation of framboidal pyrite (Yang et al., 2011; Li et al., 2016). With the dissolution or shedding of the pyrite crystals, honeycomb-like pyrite moulage pores were formed on the graptolite-derived OM, which were found to be very common under the SEM (Fig. 5). These pores retained the morphology of the pyrite crystals, which displayed uniform pore sizes of between 300 and 400 nm (Figs. 5b, 5c, 5e). In a previous related study, Locuks (2012) considered that the intergranular pores between pyrite crystals in framboids were usually isolated, which may potentially provide storage spaces for shale gas. However, the observed poor connectivity was

not conducive to shale gas seepage. The detailed observations of the residual moulage pores under SEM revealed that pyrite crystals were embedded in the graptolite-derived OM. That is to say, the main component of the moulage pore walls was OM, in which numerous nanopores had developed. In this study, the enlarged views of the moulage pores showed that the nanometer-sized pores were well developed in the moulage pore walls. These displayed elliptical or rounded cross sections with smooth pore walls, and the pore sizes generally ranged from 10 nm to 50 nm (Figs. 5c, 5f).

3.3.2 Organic gas pores

In addition to the OM pores in the residual moulage pore walls, nanoscale OM pores were also locally developed on the graptolite periderm (Figs. 5g, 5h, 5i). The shapes of these OM pores were elliptical or rounded, with pore sizes ranging from 10 nm to 50 nm (Fig. 5i),

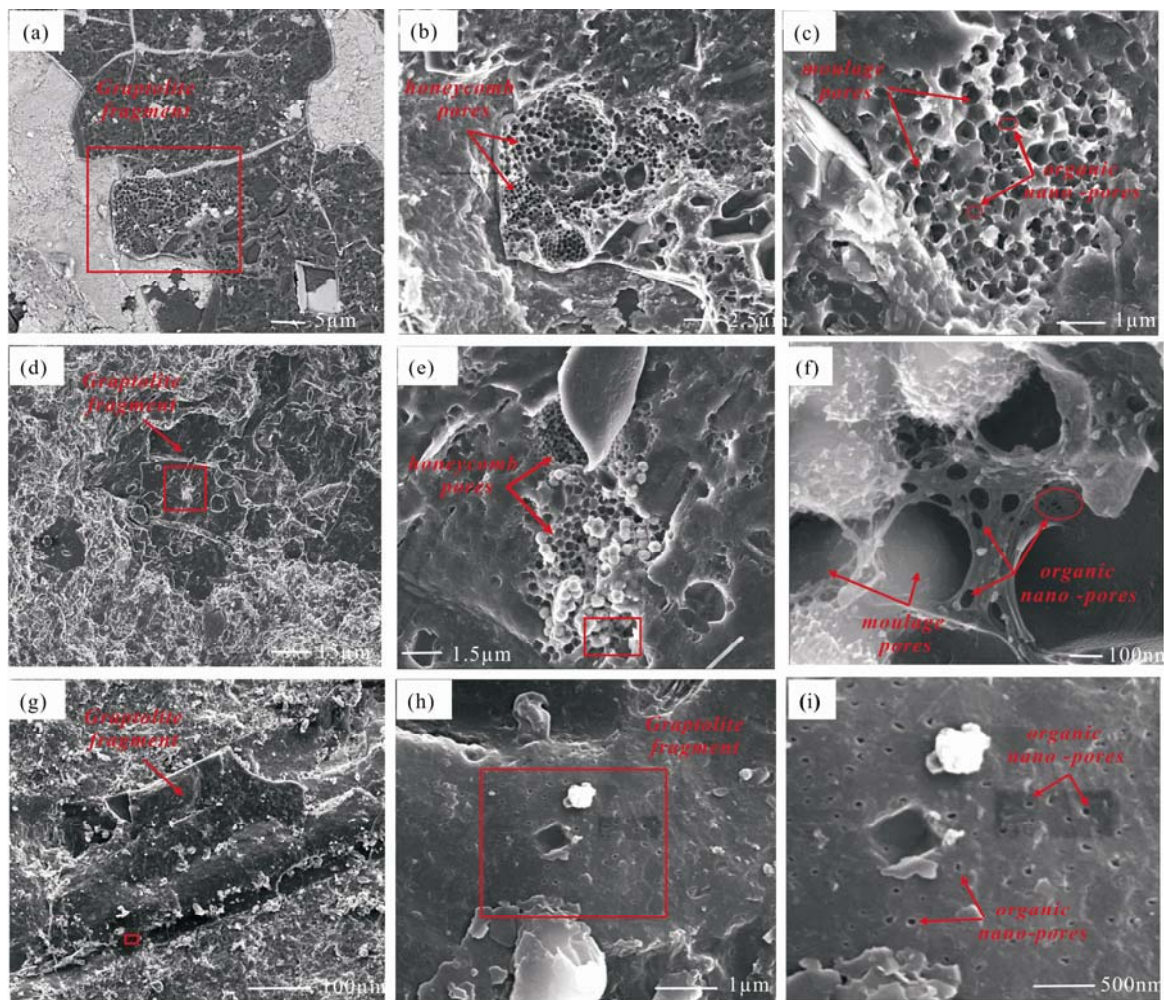


Fig. 5. Framboidal pyrite moulage pores and Organic pores of graptolites parallel to the bedding.

(a), (d) and (g) Graptolite fragments (BSE images for samples YJ1-04, WX2-04, and YJ1-01, respectively); (b) enlargement of the red frame area shown in (a) displaying the numerous honeycomb-like pyrite moulage pores on the graptolite periderm of YJ1-04; (c) Framboidal pyrite moulage pores and organic nanopores developed on the graptolite periderm of WX2-04; (e) enlargement of the red frame area shown in (d) displaying the numerous honeycomb-like pyrite moulage pores on the graptolite periderm of WX2-04; (f) enlargement of the red frame area shown in (e) in which the nanometer-sized OM pores were well developed in the moulage pore walls with elliptical or rounded cross sections, and the pore sizes ranged from 10 nm to 50 nm in WX2-04; (h) enlargement of the red frame area shown in (g) indicating that the nanoscale OM pores were locally developed on the graptolite periderm of YJ1-01; (i) enlargement of the red frame area shown in (h) indicating that the shapes of the OM pores were elliptical or rounded with pore sizes ranging between 10 and 50 nm in YJ1-01.

which were determined to be equivalent to dimensions of the OM pores in the moulage pores. It had been previously established that OM pores were created during hydrocarbon maturation (Loucks et al., 2009, 2012; Jarvie et al., 2007; Milliken et al., 2013; Li et al., 2017). The results of previous studies also showed that the graptolite periderm was comprised primarily of an aromatic structure with aliphatic groups, which had a certain hydrocarbon generation potential and mainly generated gaseous hydrocarbons (Bustin et al., 1989; Briggs et al., 1995; Gupta et al., 2006; Shen et al., 2016). In this study, it was found that the OM gas pores on the graptolite periderm were dispersed and fewer, and were different from the abundant honeycomb nanopores in the sapropel detritus. These results indicated that the graptolite may have had a certain hydrocarbon-generation potential at low maturation, but its ability to generate hydrocarbons may

have been limited.

3.3.3 Authigenic quartz moldic pores

Figs. 6a and 6d show fragments of the graptolite-derived OM under the BSE mode in this study, with a large number of micro-scale pores developed on the fragments. During the experimental process, after selecting the observational range of a small area, the pore characteristics were observed in detail under the SE mode. The results revealed that the micro-scale pores were actually not organic gas pores. They determined to be crystal-mold pores formed by partial or complete dissolution of crystals. Meanwhile, the crystal dissolution moldic pores have commonly taken the shape of the precursor. The graptolite-derived OM often coexisted with authigenic quartz, and a large amount of moldic intraP pores were left on the graptolite periderm. The diameters

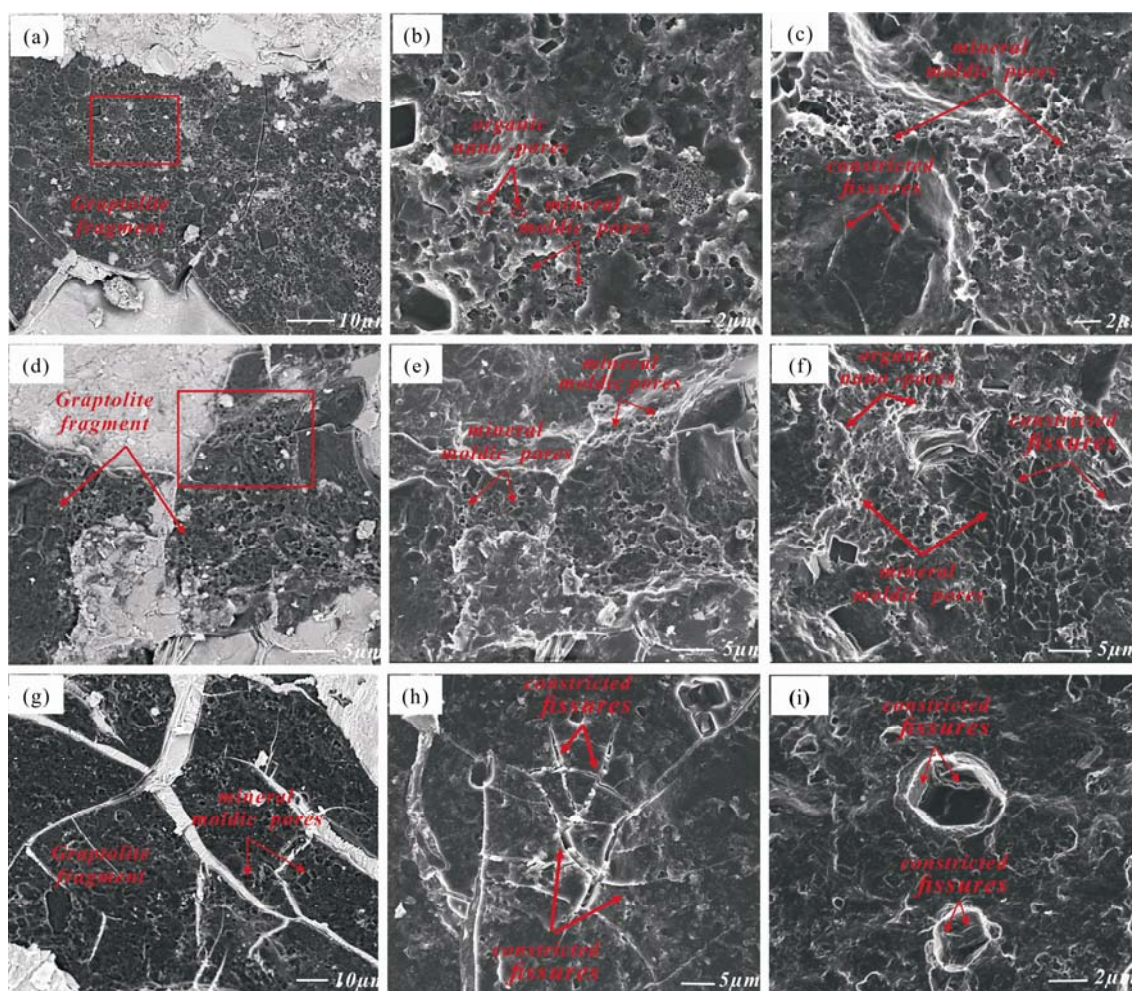


Fig. 6. Authigenic quartz moldic pores and Micro-fractures of graptolites parallel to the bedding.

(a), (d) and (g) Graptolite fragments under BSE; (a) large number of micro-scale pores developed on the graptolite periderm of YJ1-04; (b) enlargement of the red frame area shown in (a), in which the micro-scale pores are actually crystal dissolution moldic pores, which usually take the shape of quartz crystals in YJ1-04; (c) large number of crystal-mold pores coexisting with organic gas pores and densely distributed in honeycomb-like formations in YJ1-04; (d) large number of micro-scale pores developed on the graptolite periderm of YJ1-04; (e) enlargement of the red frame area shown in (d), in which the micro-scale pores have commonly taken the shape of the quartz crystals in YJ1-04; (f) crystal-mold pores remaining on the graptolite periderm, with a diameter range from hundreds of nanometers to several micrometers in YJ1-04; (g) a few micrometers to tens of micrometers of constricted fissures were generated between the graptolite fragments of WX2-04; (h) constricted fissures developed within the graptolite fragments, with widths ranging from hundreds of nanometers to several micrometers in WX2-04; (i) organic constricted fissures in the crystal dissolution moldic pores.

ranged from hundreds of nanometers to several micrometers, which had taken the shape of quartz crystals in the majority of cases (Figs. 6b, 6c, 6e, 6f). The dissolution-moldic intraP pores were the most common pore types observed on the graptolite periderm under SEM in this study.

3.3.4 Micro-fractures

It was observed that the micro-fracture networks were well-developed in the graptolite-derived OM. Since the planktonic graptolites had sunken to the seafloor after death, the periderms were much more decay resistant than the zooids, and were usually preserved as organic material (Bjerreskov, 1991; Briggs et al., 1995; Gupta et al., 2006, 2011). During the diagenetic compaction processes, the organic material became polycondensed and consolidated, which resulted in volume reduction and shrinkage (Guo et al., 2014b). Then, a few micrometers to tens of micrometers of constricted fissures were generated or within the graptolite fragments (Figs. 6g). As can be seen in Fig. 6h, constricted fissures had also developed within the graptolite fragments, with widths of approximately hundreds of nanometers to several micrometers. These organic constricted fissures could also be observed in the crystal dissolution moldic pores (Fig. 6i).

3.4 Organic gas pore structures in the graptolites obtained using FIB-slicing

After detailed observations were made of the two-dimensional pore structures of the graptolite-derived OM, the representative graptolite fragments were selected as

the target areas. A focused 30 kV beam of gallium ions was used to vertically cut the fragments, and then the new milled shale surfaces were imaged by the SEM. Fig. 7 details the internal microstructures of the sliced graptolite periderms and sapropel detritus. On the section perpendicular to bedding, it can be seen that the graptolites appeared as thin elongated bodies with the thickness of approximately 5 to 8 microns (Figs. 7a, 7d). A certain number of nanoscale gas pores were found in the graptolite-derived OM, which displayed the characteristics of flat or needle holes, and it was generally smaller than 30 nm (Figs. 7b, 7c). Along with the graptolite periderms, the sapropel detritus with smaller sizes were observed in the section (Fig. 7d). The sapropel detritus had developed numerous nanoscale pores which honeycomb-like appearances, with pore sizes ranging from 10 nm to 80 nm (Fig. 7e, 7f). It was obvious in this study that the nanoscale pores in the sapropel detritus were more developed than those in the graptolite-derived OM, and displayed better connectivity and larger diameters.

In order to quantitatively analyze the pore structures of the graptolite-derived OM and sapropel detritus, several representative high-resolution SEM images were processed in this study using Image Avizo Fire 8.0 software. The statistical data showed that the surface porosity of the graptolite-derived OM ranged from 1.5% to 2.4%, with an average value of 1.88%. Meanwhile, the surface porosity of the sapropel detritus was found to range from 3.1% to 6.2%, with an average value of 5.1%. Fig. 8 shows the histograms of the pore size distributions of the graptolite periderm (Fig. 8a) and sapropel detritus

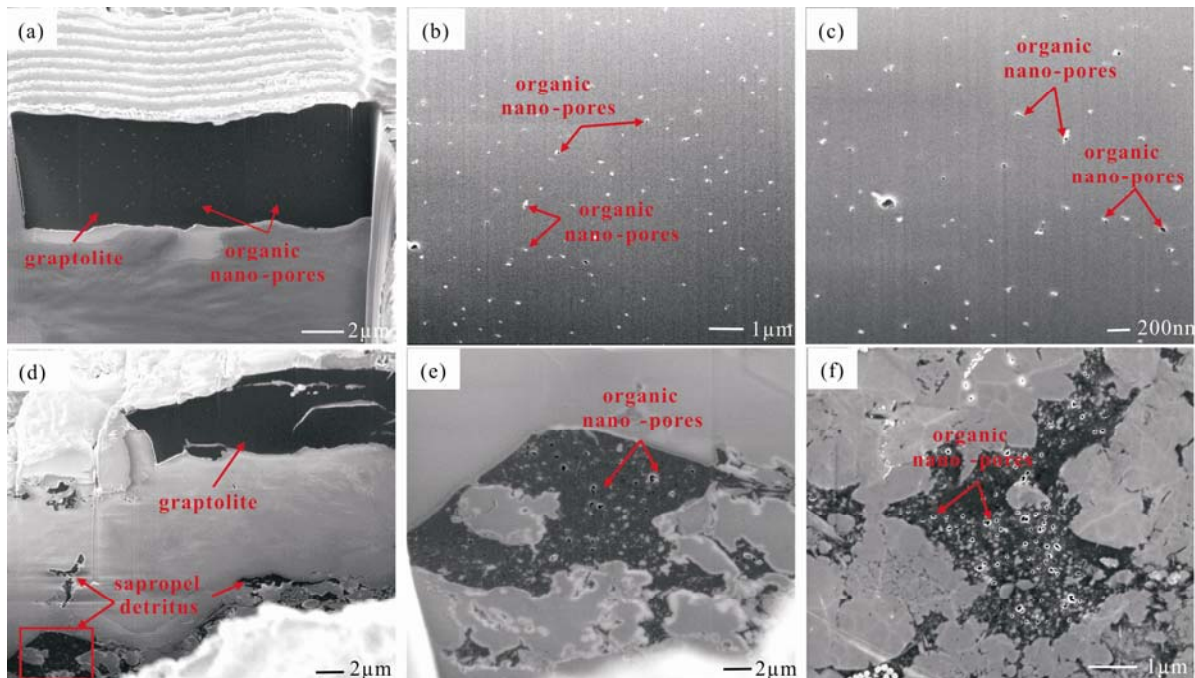


Fig. 7. Focused ion beam-scanning electron microscopy (FIB-SEM) images of sliced graptolite periderms and sapropel detritus perpendicular to the bedding.

(a) Graptolites appearing as thin elongated bodies, with thicknesses of 5 to 8 microns in WX2-05; (b) nanoscale gas pores in the graptolite periderm of WX2-05; (c) flat or prihole shaped OM pores, less than 30 nm in diameter in WX2-05; (d) sapropel detritus and graptolite periderms existing on the same longitudinal section in WX2-01; (e) enlargement of the red frame area shown in (d), indicating sapropel detritus developed on numerous nanoscale pores, with pore sizes ranging from 10 to 80 nm in WX2-01; (f) large number of bubble-like, elliptical or rounded OM pores developed in the sapropel detritus on the section parallel to the bedding in WX2-01.

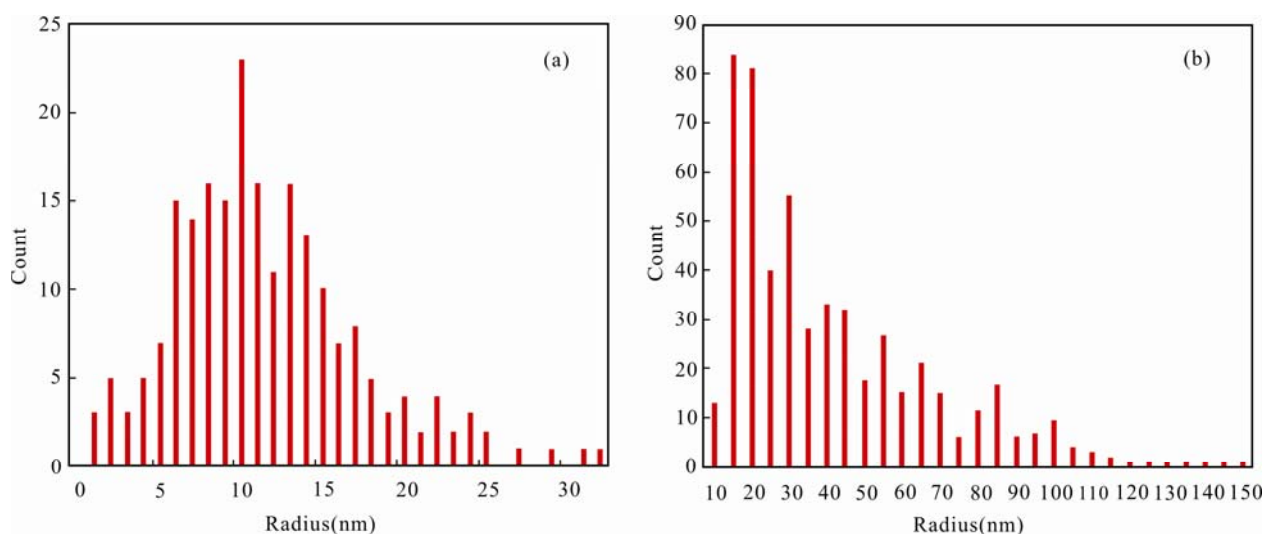


Fig. 8. Pore size distribution histograms of the OM from representative SEM images analyzed using Image Avizo Fire 8.0 software.

(a) Histograms of the pore size distributions of the graptolite periderm; (b) histograms of the pore size distributions of the sapropel detritus grains.

grain (Fig. 8b), respectively. It can be seen in the figure that the pore diameters of the graptolite-derived OM ranged from 2 nm to 40 nm, and were concentrated between 5 and 20 nm. Meanwhile, the pore diameters of the sapropel detritus were determined to range from 10 nm to 150 nm, and were concentrated between 20 and 80 nm. The results of the quantitative analysis illustrated that there was a difference between the graptolite periderms and sapropel detritus in the WF-LMX Fm shale. In summary, the sapropel detritus displayed a wider pore size distribution range and larger surface porosity when compared with the graptolite periderms.

4 Discussions

4.1 Contribution of the graptolite-derived OM to the total OM

Along with the zooplankton (for example, graptolites), planktonic algae were also important biological sources of marine sediment during the Lower Paleozoic Period (Qin et al., 2014; Shen et al., 2016; Wei et al., 2017; Tenger et al., 2017). Therefore, numerous discrete porous OM with much smaller sizes were also observed in the WF-LMX Fm shale. These were found to usually have atypical residual biostructures, and were possibly derived from planktonic algae. In this study, these discrete OM were considered to be sapropel detritus. After detailed observations of the graptolite-derived OM were completed, the samples were polished using dry emery paper for the purpose of observing the distributions of the sapropel detritus more clearly within the same field of view. Fig. 9 details this study's comparison results of the distributions of the OM in the graptolites and surrounding rock (Figs. 9a, 9d). The upper left section of the figure indicates the distributions of the graptolite fragments, and the lower right section denotes the distributions of the sapropel detritus in surrounding rock. Then, in order to quantitatively analyze the proportions of the OM in the graptolites and surrounding rock, the SEM images were

processed using Image Avizo Fire 8.0 software. The results demonstrated that the proportion of the OM in the graptolite ranged from 19.7% to 40.5% (Figs. 9b, 9e), and while the proportion of the sapropel detritus in surrounding rock was between 11.3% and 14.2% (Figs. 9c, 9f). These results indicated that the content of OM in the graptolites was greater than that in the surrounding rock. Moreover, on the bedding surfaces which contained graptolites, the graptolite-derived OM accounted for between 58% and 75% of the total OM (Figs. 9a, 9d). The graptolite-bearing shale samples which were used in this study had been selected from the Katian to the Aeronian biozones, and TOC content analyses of the graptolites and surrounding rock on the same surface layers had been carried out for each sample. This study's experimental results are detailed in Table 1. It was found that in all of the shale samples, the TOC content of the graptolites was higher than that of the surrounding rock. Consequently, the experimental results suggested that the graptolite-derived OM in the WF-LMX Fm shale had made significant contributions to the total organic matter.

4.2 Contribution of the graptolites to the shale gas generation

The results of the previous studies have suggested that the chemical composition of the graptolite periderm was dominated by aliphatic components, and the hydrogen and oxygen indices of the graptolites periderm were similar to Type II kerogen (Bustin et al., 1989; Gupta et al., 2006). Shen et al. (2016) and Wang et al. (2017) had performed Py-GC analyses on extracted low maturity graptolites from the WF-LMX Fm. The results indicated that the pyrolysis hydrocarbon products were mainly composed of natural gas and light oil, and the amounts of gaseous hydrocarbons were more than half of the total hydrocarbons. These findings indicated that the graptolites had certain hydrocarbon-generation potential. In the current study, an FIB gallium ion beam was used to vertically cut the graptolite samples. The results indicated

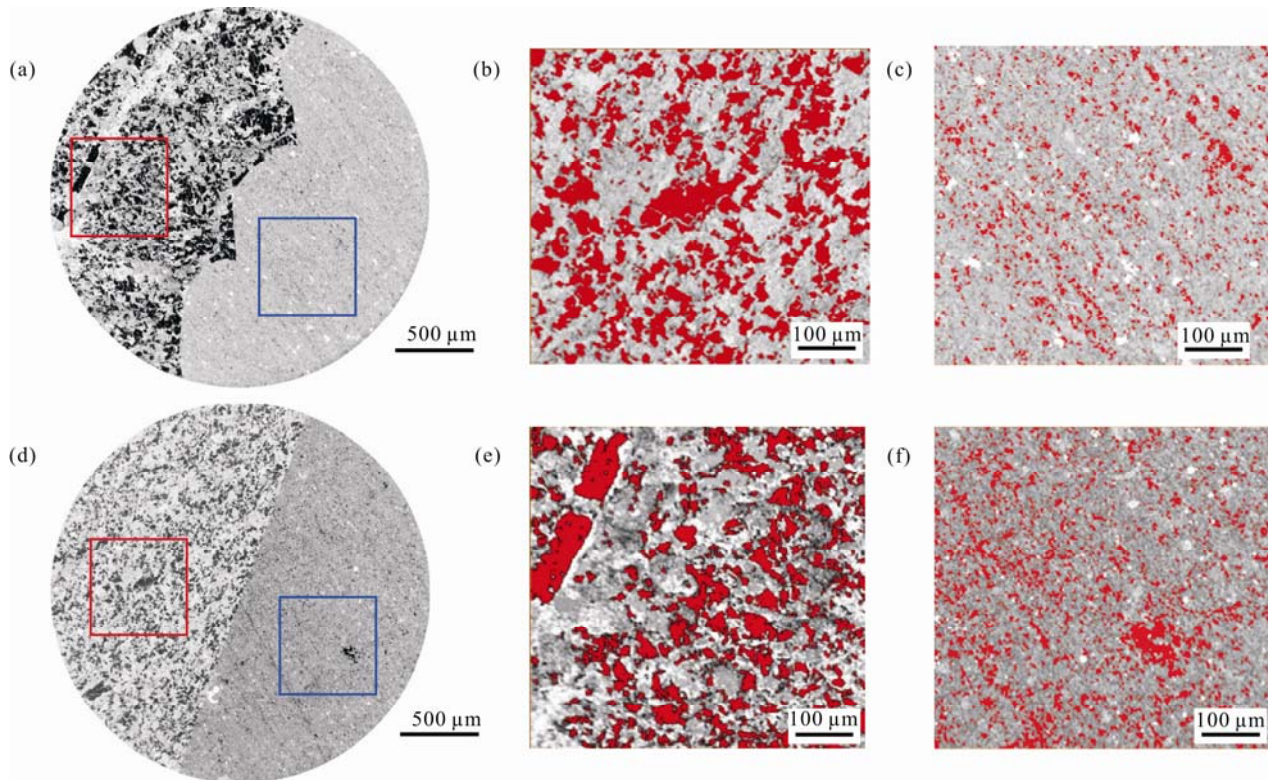


Fig. 9. Comparison of the distributions of the OM in the graptolites and surrounding rock.

(a) Comparison of the distributions of the OM in the graptolites and surrounding rock of WX2-05; (b) enlargement of the red frame area shown in (a) displaying the mapping scan of the graptolite and extraction of organic matter (red); (c) Enlargement of the blue frame area shown in (a) displaying the mapping scan of the surrounding rock and the extraction of the organic matter (red); (d) comparison of the distributions of the OM in the graptolites and surrounding rock of WX2-04; (e) enlargement of the red frame area shown in (d) displaying the mapping scan of the graptolite and the extraction of the organic matter (red); (f) enlargement of the blue frame area shown in (d) displaying the mapping scan of the surrounding rock and the extraction of the organic matter (red).

Table 1 Basic information for the shale core samples from the study area

Wells	Samples	Depth (m)	Graptolite zones	TOC of the graptolite (%)	TOC of the surrounding rock (%)
WX2	WX2-05	1568	LM8	3.10	2.93
YJ1	YJ1-06	1440	LM7	1.10	1.07
WX2	WX2-04	1610.86	LM6	4.10	4.00
WX2	WX2-03	1613.86	LM4-5	5.41	4.59
YJ1	YJ1-05	1525.56	LM4-5	3.14	2.91
YJ1	YJ1-04	1531.46	LM3	4.52	3.73
YJ1	YJ1-03	1537.16	LM2	6.66	6.51
WX2	WX2-02	1623.12	LM1	6.60	5.70
WX2	WX2-01	1630.30	WF2-3	6.50	6.10
YJ1	YJ1-01	1542.66	WF2-3	4.50	4.16

that only a certain amount of nanoscale gas pores were located inside the graptolite. These pores were observed to be flat or needle holes, with a diameters ranging from 2 nm to 40 nm (Fig. 8a). However, the nanoscale pores in sapropel detritus on the same section were observed to be obviously more developed than those in the graptolite, and had diameters ranging between 10 nm and 80 nm (Fig. 8b). Meanwhile, on the section parallel to the bedding, SEM observations also showed that a large number of bubble-like, elliptical or rounded organic matter pores were developed in the sapropel detritus, with the pore sizes ranging between 20 and 130 nm (Fig. 7f).

The differences in the organic pores of the graptolite

periderms and the sapropel detritus may have been caused by variations in the hydrocarbon generation capacities of the two types of microscopic components. The planktonic algae is a kind of hydrogen-rich organic material composed of aliphatic structures, and usually has higher hydrocarbon generation potential (Qin et al., 2014; Tenger et al., 2017). During the processes of hydrocarbon generation, large numbers of pores may have been generated, which would have resulted in abnormally high pressure conditions. These conditions would have been sufficient to support the overlying formation pressures, and the OM pores could have been retained. The main component of the graptolites was an aromatic structure with aliphatic groups, which was characterized by low hydrogen content and high aromaticity (Bustin et al., 1989; Wei et al., 2015; Tenger et al., 2017), resulting in poor hydrocarbon generation abilities in the graptolites. Therefore, it was concluded that the graptolite periderm could have produced lower pore-volumes from the decomposition of the OM, which would have made it difficult to support the overlying pressures. These factors may have caused the internal organic pores of the graptolite to be compacted or collapsed. Also, the pore outlines became unclear, and pore sizes became too small for the SEM to detect. In summary, due to the low hydrogen content and high aromaticity of the graptolites, they could not effectively provide the main source for the

shale gas. This indicated that the contribution of the graptolites to the total gas content of the shale was relatively limited.

4.3 Contribution of the graptolites to the shale gas reservoirs

The authigenic quartz moldic pores were the most common type of pores observed on the graptolite periderm in this study. In previous related studies, Wang et al. (2014) and Zhao et al. (2017) considered that the majority of the quartz in the WF-LMX Fm shale was biogenic in origin, and may have originated from biogenic silica dissolution and recrystallization. During the Lower Paleozoic period, the planktonic shells were usually siliceous, and the microcrystalline quartz in the shale may have evolved from various plankton debris during diagenesis processes. Planktonic graptolite was found to be the most common organism in Ordovician-Silurian marine sediment. Following the deaths of the graptolites, the dissolution and re-crystallization of the biogenic silica may have led to the precipitation of authigenic microcrystalline quartz on the graptolite periderm (Zhao et al., 2016, 2017). Generally speaking, the nano-scale authigenic quartz and graptolite-derived OM were embedded and encased within each other to form interlaced structures similar to magmatic rock. This indicated that both had originated from lower organisms (for example, graptolites). During the diagenesis processes, chemical differentiations occurred between the two and separated them, respectively (Zhang et al., 2016). Then, the graptolite-derived OM was polycondensed and consolidated, and the volumes were reduced. This resulted in gaps between the quartz crystals, which caused the quartz crystals to fall off easily. This study's SEM images of the graptolite-derived OM demonstrated that a large number of crystal-mold pores coexisted with the organic gas pores. These were densely distributed in honeycomb-like formations, which subsequently had formed interconnected organic pore systems with non-negligible gas storage (Figs. 6c, 6f). In addition, the honeycomb-like pores formed by the dissolution of the pyrite crystals were also very common in the graptolites, with pore sizes varying from 300 to 400 nm (Figs. 5b, 5c). In the majority of cases, the pyrite crystals were found to be completely detached, which indicated that such pores may not have been produced during the preparation processes. It is worth noting that numerous nanoscale organic pores were also observed on the walls of the moulage pores, with the pore sizes ranging from 10 to 50 nm (Fig. 5f). These OM pores were able to effectively connect each of the moulage pores, which not only provided reservoir space for gas, but also facilitated the flow of the shale gas.

During the diagenesis processes, the organic material was polycondensed and consolidated, which caused constricted fissures between the graptolite fragments (Figs. 6g, 6h). When compared with the internal pores in the graptolite-derived OM, these intricate microfractures were observed to not only provide larger storage space, but also more importantly supplied interconnections between the pores to form effective shale gas flow channels (Ma et al., 2016; Zhou et al., 2017; Nie et al.,

2015, 2018). The organic-rich shale was found to be characterized by highly developed lamellation (Zeng et al., 2016). The lamellation plane was a mechanically weak surface, which was easily induced to form lamellation fractures during the diagenesis (Zhu et al., 2015; Tenger et al., 2017). The graptolite-bearing shale of the WF-LMX section displayed a subtle bedding structure, and large amounts of graptolite were found within the lamellar distribution, with the layer intervals of between 0.2 and 0.5 mm. Also, there were stacked graptolites observed in each layer (Fig. 3c). This unique accumulation of graptolite-derived OM caused the lamellation fractures to be open more easily, which then connected the organic and inorganic pores to form shale gas flow channels. Therefore, this was of great significance to the output of shale gas, and was a key factor for the high yield of shale gas in the WF-LMX Fm.

5 Conclusions

In this research study, a series of laboratory experiments were performed in order to investigate the graptolite-derived organic matter and pore structures of WF-LMX black shale. The following key conclusions were reached:

(1) The results of the Benchtop-SEM imaging revealed that the proportion of OM in the graptolites ranged between 19.7% and 40.5%. Meanwhile, the proportion of sapropel detritus in the surrounding rock ranged from 11.3% to 14.2%. The graptolites were found to account for between 58% and 75% of the total OM in the WF-LMX Fm. The TOC content of the graptolites was determined to be higher than that of the surrounding rock, which indicated that the graptolites were a significant source of OM in the shale.

(2) This study's FIB-SEM observation results showed that four types of pores were developed on the graptolite periderm. These included organic pores, pyrite moulage pores, authigenic quartz moldic pores, and microfractures. These well-developed micro-nano pores and fractures had formed an interconnected system within the graptolites which provided storage spaces for shale gas. The stacked accumulations of the graptolites allowed the lamellation fractures to be open more easily, which then acted as flow pathways for the shale gas.

(3) The results of this study's ion beam milling experiment revealed that there were a small number of nanoscale gas pores in the graptolites, with surface porosity between 1.5% and 2.4%, and pore diameters ranging from 5 to 20 nm. Meanwhile, the sapropel detritus was observed to be rich in nanometer-sized pores with surface porosity of 3.1% to 6.2%, and pore diameters ranging between 20 and 80 nm. The gas pores in the graptolites displayed smaller pore size distribution ranges and surface porosity. The differences in the organic pores of the graptolite periderms and sapropel detritus indicated that the compositions of the OM may have been an important factor controlling the OM pore development.

Acknowledgements

This study was supported by the National Science and

Technology Major Project of China (Grant No. 2017ZX05035-001).

Manuscript received Sept. 20, 2018
accepted Dec. 20, 2018
associate EIC HAO Ziguo
edited by LIU Lian

References

- Baliński, A., and Sun, Y.L., 2013. Preservation of soft tissues in an Ordovician linguloid brachiopod from China. *Acta Palaeontologica Polonica*, 58(1): 115–120.
- Bjerreskov, M., 1991. Pyrite in Silurian graptolites from Bornholm, Denmark. *Lethaia*, 24: 351–361.
- Borjigin Tenger., Shen, B.J., Yu, L.J., Yang, Y.F., Zhang, W.T., Tao, C., Xi, B.B., Zhang, Q.Z., Bao, F., and Qin, J.Z., 2017. Mechanisms of shale gas generation and accumulation in the Ordovician Wufeng-Longmaxi Formation, Sichuan Basin, SW China. *Petroleum Exploration and Development*, 44(1): 69–78.
- Bustin, R.M., Link, C., and Goodarzi, F., 1989. Optical properties and chemistry of graptolite periderm following laboratory simulated maturation. *Organic Geochemistry*, 14: 355–364.
- Briggs, D.E.G., Bottrell, S.H., and Raiswell, R., 1991. Pyritization of soft-bodied fossils: Beecher's Trilobite Bed, Upper Ordovician, New York State. *Geology*, 19(12): 1121–1124.
- Briggs, D.E.G., Kear, A.J., Baas, M., de Leeuw, J.W., and Rigby, S., 1995. Decay and composition of the hemichordate *Rhabdopleura*: implications for the taphonomy of graptolites. *Lethaia*, 28: 15–23.
- Chen, X., Fan, J.X., Melchin, M. J., and Mitchell, C.E., 2005. Hirnantian (latest Ordovician) graptolites from the Upper Yangtze region, China. *Palaeontology*, 48: 235–280.
- Chen, X., Fan, J.X., Zhang, Y.D., Wang, H.Y., Chen, Q., Wang, W.H., Liang, F., Guo, W., Zhao, Q., Nie, H.K., Wen, Z.D., and Sun, Z.Y., 2015. Subdivision and delineation of the Wufeng and Lungmachi black shales in the subsurface areas of the Yangze Platform. *Journal of Stratigraphy*, 39(4): 351–358 (in Chinese with English abstract).
- Chen, X., Melchin, M.J., and Sheets, H.D., 2005. Patterns and processes of latest Ordovician graptolite extinction and recovery based on data from south China. *Journal of Paleontology*, 79(5): 842–861.
- Chen, X., Fan, J.X., Melchin, M.J., and Mitchell, C.E., 2005b. Hirnantian (latest Ordovician) graptolites from the Upper Yangtze region, China. *Palaeontology*, 48(2): 235–280.
- Chen, X., Rong, J.Y., Li, Y., and Boucot, A.J., 2004. Facies patterns and geography of the Yangtze region, South China, through the Ordovician and Silurian transition. *Palaeogeography, Palaeoclimatology, Palaeoecology*, 204(3): 353–372.
- Chen, X., Rong, J.Y., Mitchell, C.E., Harper, D.A.T., Fan J.X., Zhan R.B., Zhang Y.D., Li R.Y., and Wang Y., 2000b. Late Ordovician to earliest Silurian graptolite and brachiopod biozonation from the Yangtze region, South China with a global correlation. *Geological Magazine*, 137(6): 623–650.
- Crowther, P.R., 1981. The fine structure of graptolite periderm. *Special Papers in Palaeontology*, 26(93): 1–119.
- Dai, N., Zhong, N.N., Zhang, Y., Zhang, W., Zhao, J., and Yan, W.H., 2015. Ar ion milling/SEM analysis on graptolite macerals. *Journal of Chinese Electron Microscopy Society*, 34: 416–420 (in Chinese with English abstract).
- Dong, D.Z., Shi, Z.S., Guan, Q.Z., Jiang, S., Zhang, M.Q., Zhang, C.C., Wang, S.Y., Sun, S.S., Yu, R.Z., Liu D.X., Peng P., and Wang S.Q., 2018. Progress, challenges and prospects of shale gas exploration in the Wufeng-Longmaxi reservoirs in the Sichuan Basin. *Natural Gas Industry*, 38(4): 67–76 (in Chinese with English abstract).
- Gupta, N.S., Briggs, D.E., and Pancost, R.D., 2006. Molecular taphonomy of graptolites. *Journal of the Geological Society*, 163(6): 897–900.
- Guo, X.S., Hu, D.F., Wen, Z.D., and Liu, R.B., Marine shale gas in the Lower Paleozoic of Sichuan Basin and its periphery: A case study of the Wufeng-Longmaxi Formation of Jiaoshiba area. *Geology in China*, 2014, 41(3): 893–901 (in Chinese with English abstract).
- Guo, X.S., Li, Y.P., Liu, R.B., and Wang, Q.B., 2014. Characteristics and controlling factors of micro-pore structures of Longmaxi Shale Play in the Jiaoshiba area, Sichuan Basin. *Natural Gas Industry*, 38(4): 67–76 (in Chinese with English abstract).
- Li, C.C., and OU, C.H., 2018. Modes of Shale-Gas Enrichment Controlled by Tectonic Evolution. *Acta Geologica Sinica (English Edition)*, 92(5): 1934–1947.
- Li, T.W., Jiang, Z.X., Li, Z., Wang, P.F., Xu, C.L., Liu, G.H., Su, S.Y., and Ning, C.X., 2017. Continental shale pore structure characteristics and their controlling factors: A case study from the lower third member of the Shahejie Formation, Zhanhua Sag, Eastern China. *Journal of Natural Gas Science and Engineering*, 45: 670–692.
- Liu, Z.Q., Liu, L., Huang, M., Fei, H.C., Zhou, J., Zhang, Y.X., and Hao, Z.G., 2018. Present Situation of China's Shale Gas Exploration and Development. *Acta Geologica Sinica (English Edition)*, 29(5): 2026–2027.
- Loucks, R.G., Reed, R.M., Ruppel, S.C., and Jarvie, D.M., 2009. Morphology, Genesis, and Distribution of Nanometer-Scale Pores in Siliceous Mudstones of the Mississippian Barnett Shale. *Journal of Sedimentary Research*, 79(12): 848–861.
- Loucks, R.G., Reed, R.M., Ruppel, S.C., and Hammes, U., 2012. Spectrum of pore types and networks in mudrocks and a descriptive classification for matrix-related mudrock pores. *AAPG Bulletin*, 96(6): 1071–1098.
- Luo, Q.Y., Zhong, N.N., Dai, N., and Zhang, W., 2016. Graptolite-derived organic matter in the Wufeng-Longmaxi Formations (Upper Ordovician-Lower Silurian) of southeastern Chongqing, China: Implications for gas shale evaluation. *International Journal of Coal Geology journal*, 153 (1-2): 87–98.
- Jarvie, D.M., Hill, R.J., Ruble, T.E., and Pollastro, R.M., 2007. Unconventional shale-gas systems: the Mississippian Barnett Shale of north-central Texas as one model. *AAPG Bulletin*, 91 (4): 475–499.
- Ma, X.H., 2017. A golden era for natural gas development in the Sichuan Basin. *Natural Gas Industry*, 37(2): 1–10 (in Chinese with English abstract).
- Ma, Y., Zhong, N.N., Cheng, L.J., Pan, Z.J., D, N., Zhang, Y., and Liu, Y., 2016. Pore structure of the graptolite-derived OM in the Longmaxi Shale, southeastern Upper Yangtze Region, China. *Marine & Petroleum Geology*, 72: 1–11.
- Milliken, K., Rudnicki, M., Awwiller, D.N., and Zhang T.W., 2013. Organic matter-hosted pore system, Marcellus Formation (Devonian), Pennsylvania. *AAPG Bulletin*, 97: 177–200.
- Mu, C.L., Ge, X.Y., Xu, X.S., Zhou, K.K., Liang, W., and Wang, X.P., 2014. Lithofacies palaeogeography of the Late Ordovician and its petroleum geological significance in Middle-Upper Yangtze Region. *Journal of Palaeogeography*, 16(4): 427–440 (in Chinese with English abstract).
- Nie, H.K., Jin, Z.J., Ma, X., Liu, Z.B., Lin T., and Yang Z.H., 2017. Graptolites zone and sedimentary characteristics of Upper Ordovician Wufeng Formation-Lower Silurian Longmaxi Formation in Sichuan Basin and its adjacent areas. *Acta Petrolei Sinica*, 38(2): 160-174 (in Chinese with English abstract).
- Nie, H.K., Jin, Z.J., and Zhang, J.C., 2018. Characteristics of three organic matter pore types in the WufengLongmaxi Shale of the Sichuan Basin, Southwest China. *Scientific Reports*, 8: 1–11.
- Nie, H.K., Zhang, J.C., and Jiang, S.L., 2015. Types and characteristics of Lower Silurian shale gas reservoirs in and around the Sichuan Basin. *Acta Geologica Sinica (English Edition)*, 89(6): 1973–1985.
- Peterson, H.I., Schovsbo, N.H., and Nielsen, A.T., 2013. Reflectance measurements of zooclasts and solid bitumen in Lower Palaeozoic shales, southern Scandinavia: correlation to

- vitrinite reflectance. *International Journal of Coal Geology*, 114(4): 1–18.
- Qin, J.Z., Shen, B.J., Tao, G.L., Borjigin Tenger, Yang, Y.F., Zheng, L.J., and Fu, X.D., 2014. Hydrocarbon-forming organisms and dynamic evaluation of hydrocarbon generation capacity in excellent source rocks. *Petroleum Geology & Experiment*, 36(4): 465–472 (in Chinese with English abstract).
- Ran, B., Liu, S.G., Luba JANSAN, Sun, W., Yang, D., Wang, S.Y., Ye, Y.H., Christopher Xiao, Zhang, J., Zhai, C.B., Luo, C. and Zhang, C.J., 2016. Reservoir Characteristics and Preservation Conditions of Longmaxi Shale in the Upper Yangtze Block, South China. *Acta Geologica Sinica (English Edition)*, 90(6): 2182–2205.
- Schieber, J., Krinsley, D., and Riciputi, L., 2000. Diagenetic origin of quartz silt in mudstones and implications for silica cycling. *Nature*, 406, 981–985.
- Shen, B.J., Yang Y.F., Borjigin Tenger, Qin J.Z., and Pan A.Y., 2016. Characteristics and hydrocarbon significance of organic matter in shale from the Jiaoshiba structure, Sichuan Basin. *Petroleum Geology&Experiment*, 38(4): 480–495 (in Chinese with English abstract).
- Suchý, V., Šýkorová, I., Stejskal, M., Šafanda, J., Machovič, V., and Novotná, M., 2003. Dispersed organic matter from Silurian shales of the Barrandian Basin, Czech Republic: optical properties, chemical composition and thermal maturity. *International Journal of Coal Geology*, 53(1): 1–25.
- Towe, K.M., and Urbanek, A., 1972. Collagen-like structures in Ordovician graptolite periderm. *Nature*, 237(5356): 443–445.
- Underwood, C.J., and Bottrell, S.H., 1994. Diagenetic controls on multiphase pyritization of graptolites. *Geological Magazine*, 131(3): 315–327.
- Wang, H.Y., Guo, W., Liang, F., and Zhao, Q., 2015. Biostratigraphy characteristics and scientific meaning of the Wufeng and Longmaxi Formation black shales at well Wei 202 of the Weiyuan shale gas field, Sichuan Basin. *Journal of Stratigraphy*, 39(3): 289–293(in Chinese with English abstract).
- Wang, Q., Qian, M.H., Jiang, Q.G., Yang, Y.F., and Borjigin Tenger., 2017. A study on hydrocarbon generation capacity of graptolite in marine hydrocarbon source rocks in southern China. *Rock and Mineral analysis*, 2017,36(3): 258–264 (in Chinese with English abstract).
- Wang, S.F., Zou, C.N., Dong, D.Z., Wang, Y.M., Huang, J.L., and Guo, Z.J., 2014. Biogenic Silica of Organic-Rich Shale in Sichuan Basin and Its Significance for Shale Gas. *Acta Scientiarum Naturalium Universitatis Pekinensis*, 50(3): 476–486(in Chinese with English abstract).
- Wei, X.F., Zhao, Z.B., Wang, Q.B., Liu, Z.J., Zhou, M., and Zhang, H., 2017. Comprehensive Evaluation on Geological Conditions of the Shale Gas in Upper Ordovician Wufeng Formation-Lower Silurian Longmaxi Formation in Dingshan Area, Qijiang, Southeastern Sichuan. *Geological Review*, 63 (1): 153–164.
- Wilkin, R.T., and Barnes, H.L., 1996. Formation processes of framboidal pyrite. *Geochimica et Cosmochimica Acta*, 61(2): 323–339.
- Wu, J., Liang, F., Lin, W., Wang, H.Y., Bai, W.H., Ma, C., Sun, S. S., Zhao, Q., Song, X.J., and Yu, R.Z., 2017. Characteristics of shale gas reservoirs in Wufeng Formation and Longmaxi Formation in Well WX2, northeast Chongqing. *Petroleum Research*, 2(4): 1–12.
- Zalasiewicz, J., 2001. Graptolites as constraints on models of sedimentation across Iapetus: a review. *Proceedings of the Geologists' Association*, 112: 237–251.
- Zeng, L.B., Lyu, W.Y., Li, J. Zhu, L.F., Weng, J.Q., Yue, F., Zu, K.W., 2016. Natural fractures and their influence on shale gas enrichment in Sichuan Basin, China. *Journal of Natural Gas Science and Engineering*, 30:1–9.
- Zhai, G.Y., Wang, Y.F., Zhou, Z., Yu, S.F., Chen, X.L., and Zhang, Y.X., 2018. Exploration and research progress of shale gas in China. *China Geology*, 2, 257–272.
- Zhang, H., Li, G.H., and Jie, L.Q., 2018. Organic matters and their occurrence state in Lower Paleozoic shale in south China. *Coal Geology & Exploration*, 46(1): 51–55 (in Chinese with English abstract).
- Zhang, Y.D., and Chen, X., 2008. Diversity history of Ordovician graptolites and its relationship with environmental change. *Science in China, Series D: Earth Sciences*, 51(2): 161–171.
- Zhao, J.H., Jin, Z.J., Jin, Z.K., Hu, Q.H., Hu, Z.Q., Du, W., Yan, C.N., and Geng, Y.K., 2017. Mineral types and organic matters of the Ordovician-Silurian Wufeng and Longmaxi Shale in the Sichuan Basin, China: Implications for pore systems, diagenetic pathways, and reservoir quality in fine-grained sedimentary rocks. *Marine and Petroleum Geology*, 86: 655–674.
- Zhao, J.H., Jin, Z.J., Jin, Z.K., Wen, X., and Geng, Y.K., 2016. Physical mechanism of organic matter-mineral interaction in Longmaxi shale, Sichuan Basin, China. *Acta Geologica Sinica (English Edition)*, 90(5): 1923–1924.
- Zhou, Y. Y., Ji, Z.W., Shen, B.J., Yang, Y.F., Qiu, N.S., and Borjigin Tenger., 2017. Research progress on main controlling factor of hydrocarbon-forming organisms in gas-bearing property. *Bulletin of Mineralogy, Petrology and Geochemistry*, 36(2): 332–338.
- Zhu, Y.M., Zhang, H., Kang, W., Wang, Y. and Chen, S.B., 2015. Organic nanopores of Longmaxi and Qiongzhusi Formation in the Upper Yangtze: Biological precursor and pore network. *Natural Gas Geoscience*, 26(8): 1507–1515 (in Chinese with English abstract).
- Zou, C.N., Dong, D.Z., Wang, Y.M., Li, X.J., Huang, J.L., Wang, S.F., Guan, Q.Z., Zhang, C.C., Wang, H.Y., Liu, H.L., Bai, W.H., Liang, F., Lin, W., Zhao, Q., Liu, D.X., Yang, Z., Liang, P.P., Sun, S.S., and Qiu, Z., 2015. Shale gas in China: characteristics, challenges and prospects (I). *Petroleum Exploration & Development*, 42 (6): 753–767 (in Chinese with English abstract).
- Zou, C.N., Gong, J.M., Wang, H.Y., and Shi, Z.S., 2019. Importance of graptolite evolution and biostratigraphic calibration on shale gas exploration. *China Petroleum Exploration*, 24(1): 1–6.
- Zou, C.N., Yang, Z., Pan, S.Q., Chen, Y.Y., Lin, S.H., Huang, J.L., Wu, S.T., Dong, D.Z., Wang, S.F., Liang, F.F., Sun, S.S., Huang, Y., and Weng, D.W., 2016. Shale gas formation and occurrence in China: An overview of the current status and future potential. *Acta Geologica Sinica (English Edition)*, 90 (4): 1249–1283.

About the first and corresponding author



WU Jin, female, born in Hulunbeier City, Inner Mongolia Autonomous Region, December 1988. She graduated from the Ocean University of China in 2009, and received her master's degree from the Research Institute of Petroleum Exploration and Development (RIPED, PetroChina) in 2016. She is now an engineer of the RIPED, PetroChina. Her research focuses on the shale gas accumulation mechanisms and distribution prediction. In addition, she has been conducting experimental research related to shale gas in recent years. Corresponding address: Postbox 910, Haidian District, 100083, Beijing; Phone number: 86(0)10-83596835; E-mail: wujinouc@petrochina.com.cn.